Paper:
Chen, F., Yu, S., Yuan, Y., Wang, H. & Gagen, M. (2016). A tree-ring width based drought reconstruction for southeastern China: links to Pacific Ocean climate variability. *Boreas, 45*(2), 335-346.
http://dx.doi.org/10.1111/bor.12158

Figure from the paper.

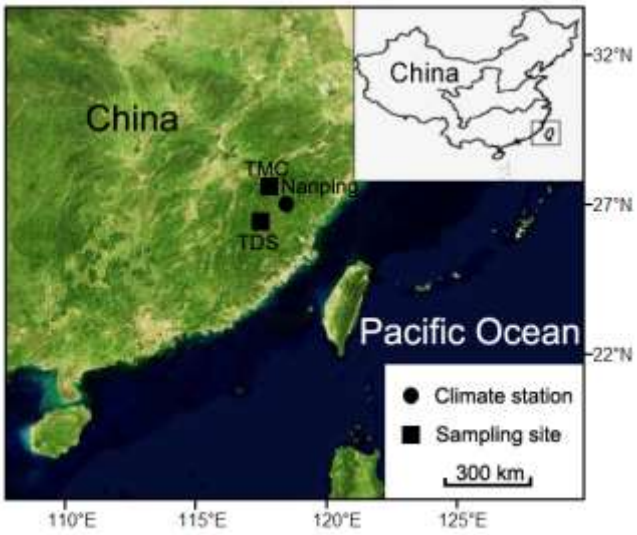

Fig. 1. Map showing the tree-ring sampling sites and the meteorological station

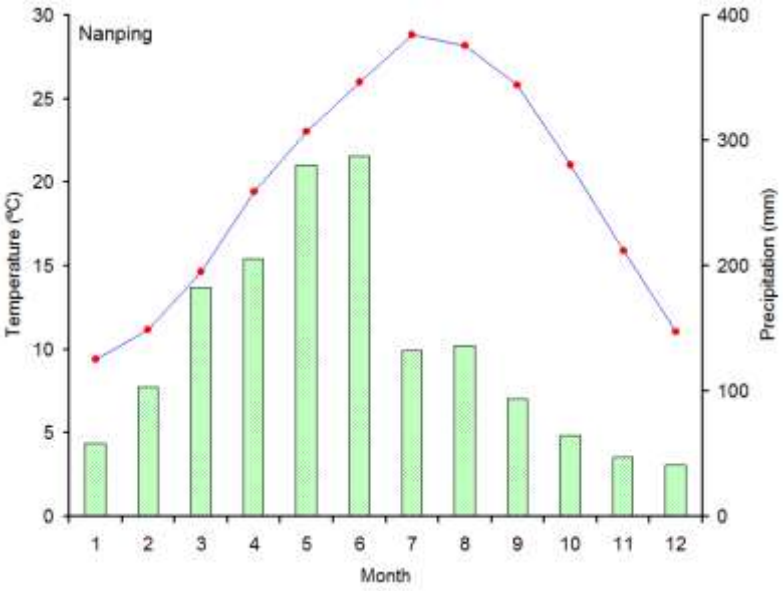

Fig. 2. Climate diagram for the meteorological station of Nanping in Fujian

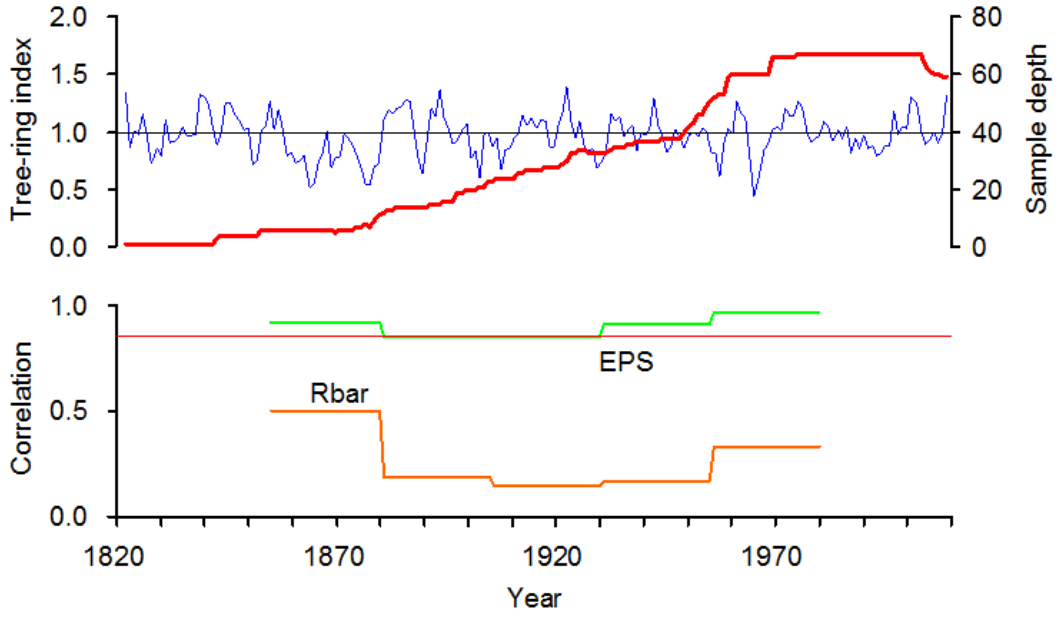

Fig. 3. Plot of the standard ring width chronology from Fujian, its running expressed population signal (EPS), sample depth and mean inter-series correlation (Rbar)

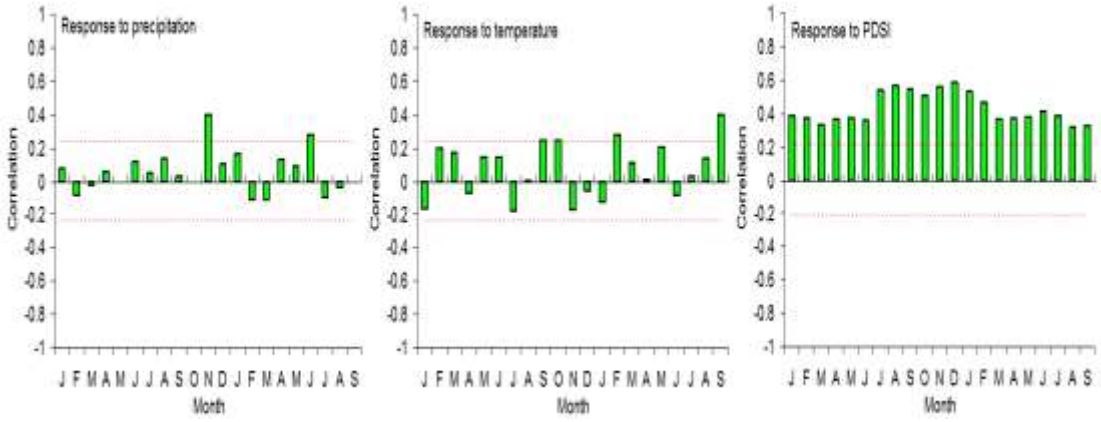

Fig. 4. Response plots for the STD chronology with monthly total rainfall, mean monthly temperature and monthly PDSI for the period 1955–2011. The coefficients were calculated from the previous year January to the current year September. Horizontal dashed lines denote 95% significance levels

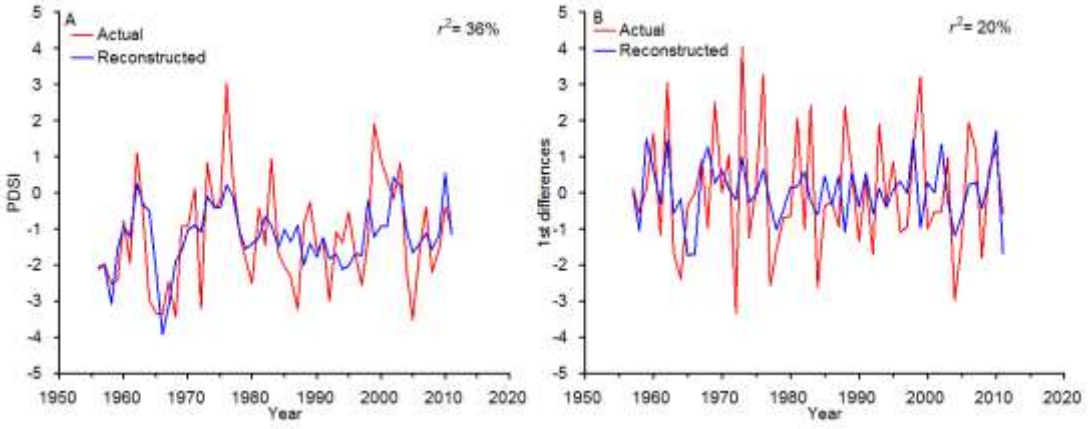

Fig. 5. (A) Comparison of actual and reconstructed July–February PDSI from 1955 to 2011. (B) Comparison between the first differences (year-to-year changes) of instrumental and reconstructed July–February PDSI for their common period 1955–2011.

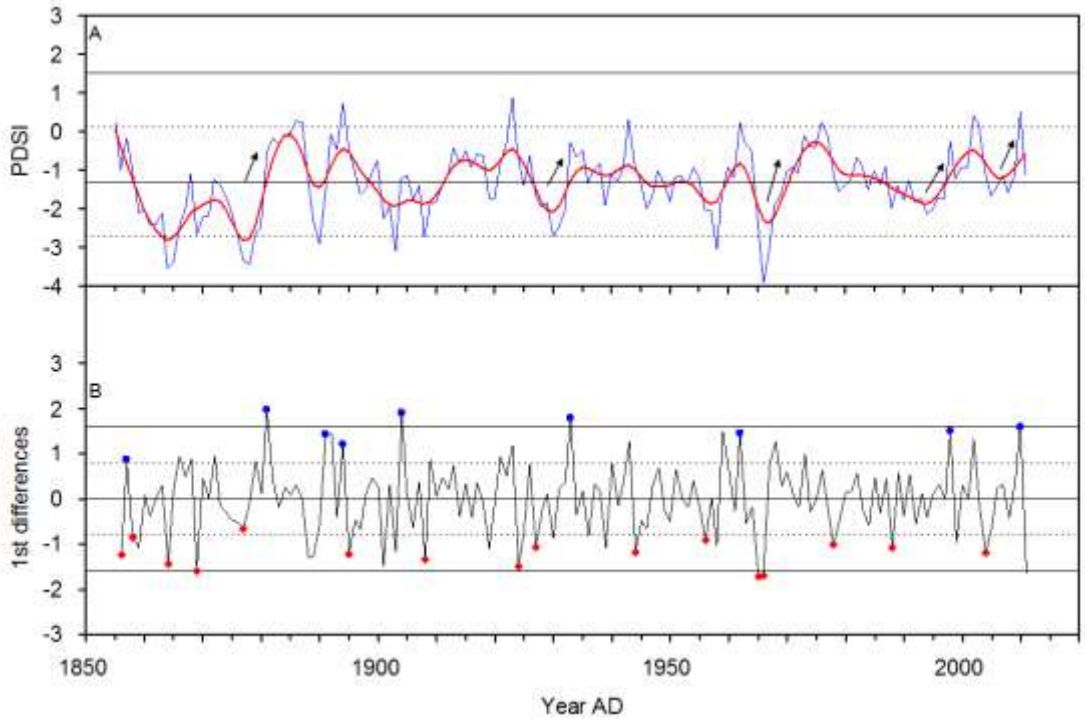

Fig. 6. (A) July–February PDSI reconstruction for central Fujian since AD 1855. The bold line indicates the smoothed data with a 10-year low-pass filter to emphasize long-term fluctuations. (B) The first differences (year-to-year changes) of the PDSI reconstruction. The central horizontal line

shows the mean of the estimated values; inner horizontal lines (dotted) shows one standard deviation; outer horizontal lines shows one standard deviation. The diamonds indicate low values, each following a drought event. The rounds indicate high values, each following a flood event.

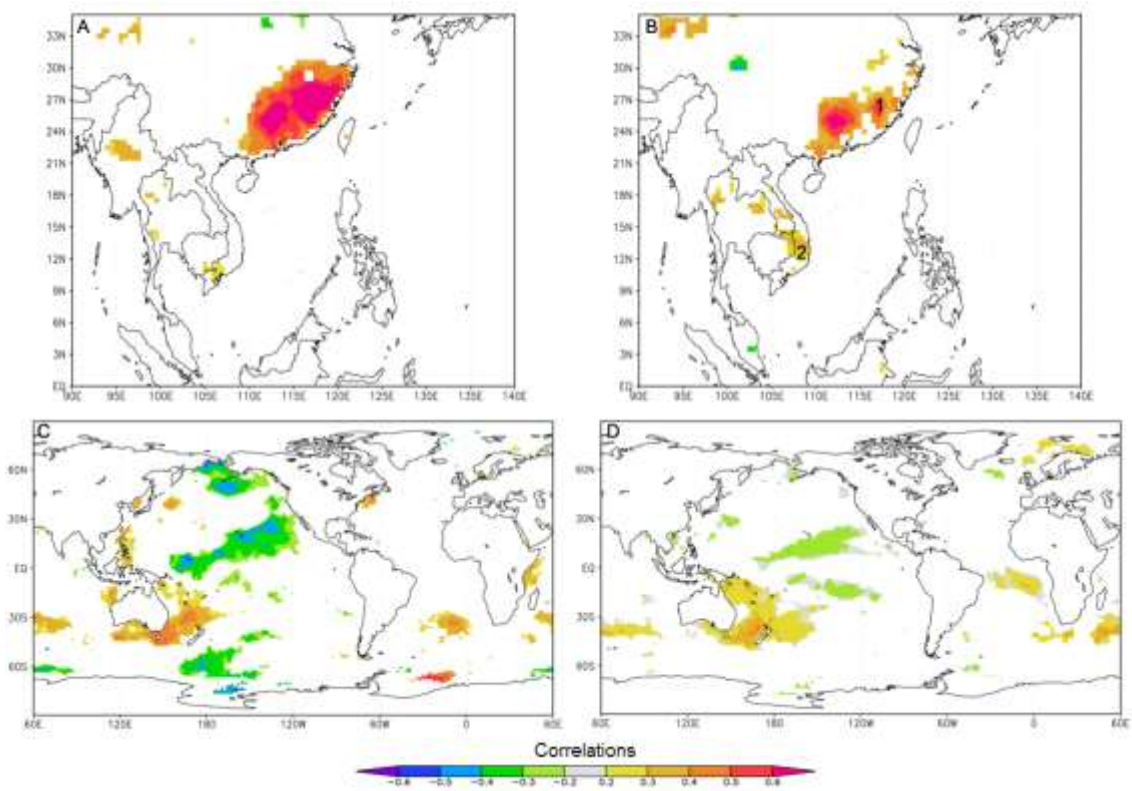

Fig. 7. Spatial correlation fields of instrumental (A) and reconstructed (B) July–February PDSI with regional gridded July–February PDSI for the period 1955–2011. The numbers 1 and 2 denote our study area and tree-ring site of Vietnam (Buckley *et al*. 2010). (B) Correlation patterns of instrumental (C) and reconstructed (D) July–February PDSI with the gridded sea surface temperature (SST) dataset of HadISST1 over their overlapping periods from 1955 to 2011 and from 1900 to 2011.

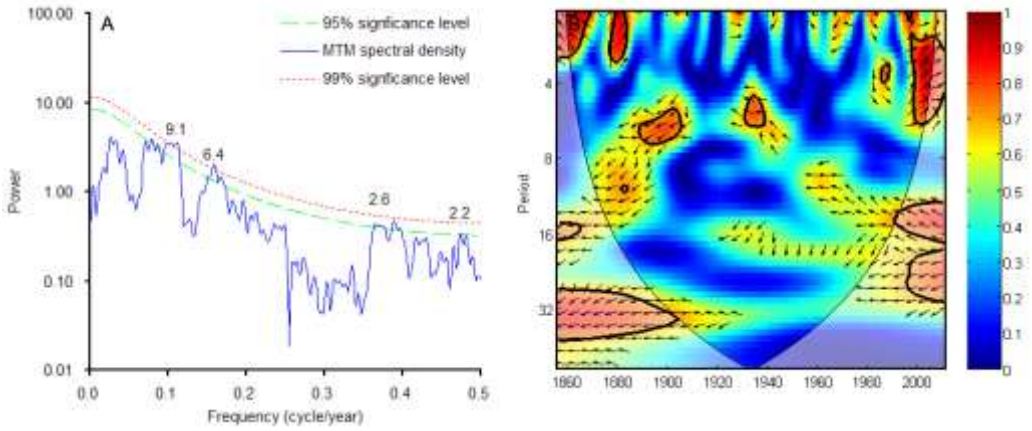

Fig. 8. (A) Results of MTM spectral analysis of the PDSI reconstruction. The dashed and dotted lines indicate the 95 and 99% significance level. (B) The wavelet coherence between the PDSI reconstruction and the ENSO index. Arrows indicate the phase of the coherence, where right is in phase and left is antiphase; note that significant regions all show an in-phase relationship, which supports the idea that there may be a simple cause and effect relationship between the two phenomena.

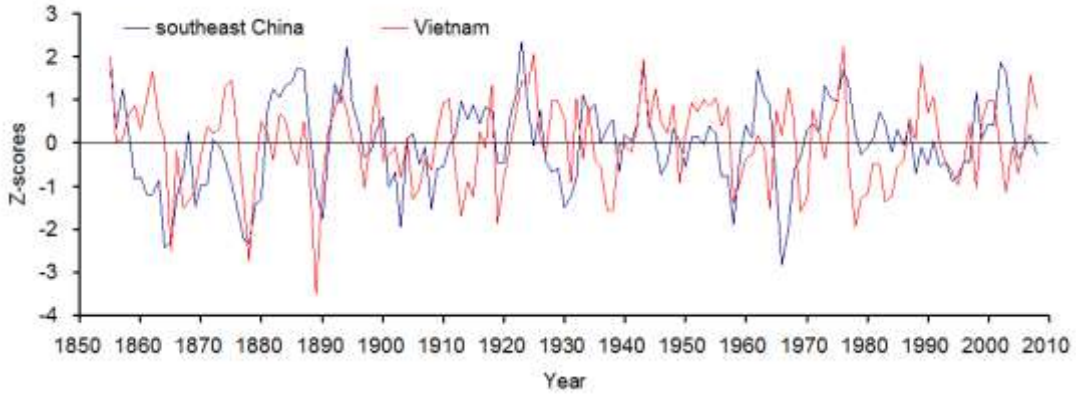

Fig. 9 Comparison of our PDSI reconstruction (southern China) and tree-ring width series of *Fokienia hodginsii* from Vietnam (Buckley *et al*. 2010).

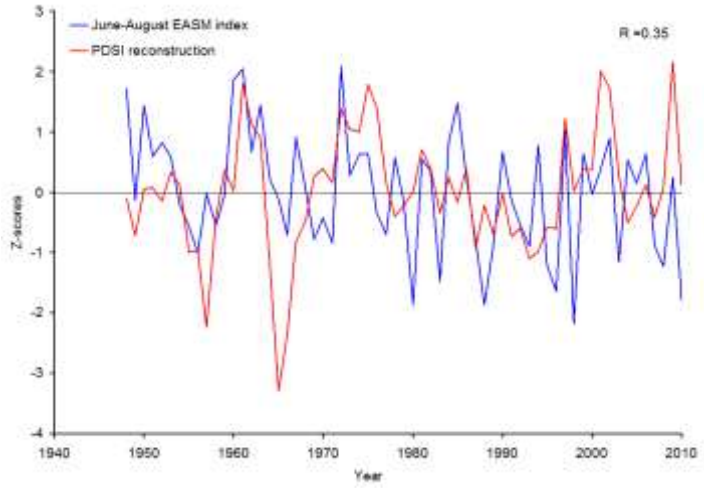

Fig. 10 Comparison of the July–February PDSI reconstruction with the June-August EASM index (Li and Zeng 2002).

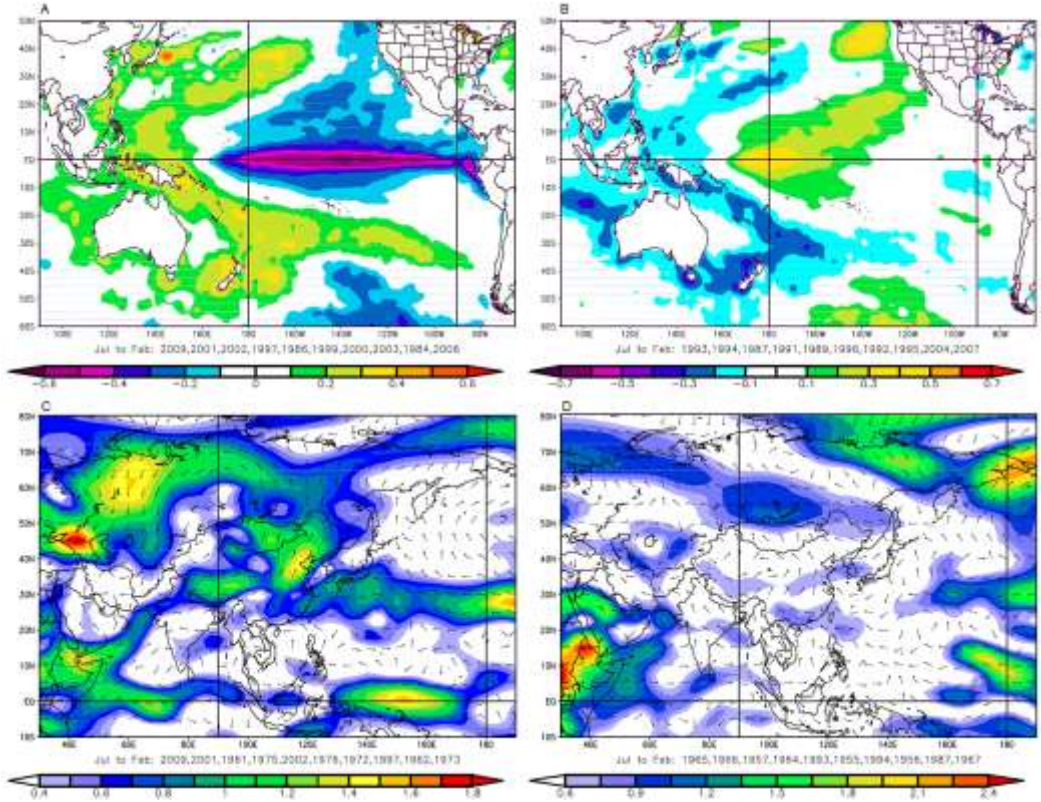

Fig. 11 Composite maps of SST for the ten wettest (A) and ten driest (B) years for southern China July–February PDSI, 1981–2011. Composite anomaly maps of 500-hPa vector wind (from July of the prior year to February of the current year) for the 10 wettest (C) and 10 driest (D) years for PDSI reconstruction during the period 1948–2008.